Appl. Phys. A 79, 1847–1851 (2004)
DOI: 10.1007/s00339-004-2939-9

Applied Physics A
Materials Science & Processing

Q. YANG[1,2,✉]
K. TANG[1,2]
J. ZUO[3]
Y. QIAN[1,2]

Synthesis and luminescent property of single-crystal ZnO nanobelts by a simple low temperature evaporation route

[1] Nano-materials and Nano-chemistry, Hefei National Laboratory for Physical Sciences at Microscale, University of Science and Technology of China (USTC), Hefei, Anhui 230026, P.R. China
[2] Department of Chemistry, University of Science and Technology of China (USTC), Hefei, Anhui 230026, P.R. China
[3] Structure Research Laboratory, Hefei National Laboratory for Physical Sciences at Microscale, University of Science and Technology of China (USTC), Hefei, Anhui 230026, P.R. China

Received: 12 May 2004/Accepted: 19 May 2004
Published online: 6 July 2004 •

ABSTRACT Large-scale ZnO nanobelts in aligned fashion have been prepared via a simply conducted low temperature evaporation route using the oxidization of metallic zinc plates at 450 ± 10 °C under ambient pressure. The produced nanobelt array has been structurally characterized by powder X-ray diffraction (XRD), scanning electron microscopy, and transmission electron microscopy (TEM). The microscope images show that the nanobelts are about 120-micron long, ranging on average from 80 to 160 micron, with about 30 nm in thickness. In addition to XRD, high-resolution TEM images and electron-diffraction patterns show that the nanobelts are single crystalline with wurtzite structure and mostly grow along the [0001] direction. The photoluminescence spectra of the single nanobelts show that the nanobelts have a dominant near-band-edge emission at about 388 nm with a very weak defect emission band centered at about 514 nm.

PACS 81.05.Ys; 81.15.Gh; 78.66.Jg

1 Introduction

The study of one-dimensional (1D) nanoscale structures has advanced rapidly over the last decade as a variety of interesting properties and possible applications result from the geometric configurations and dimensional confinements [1–9]. Examples of these properties are those of electrical, optical, magnetic, and chemical ones, tuned by the chemical compositions, radial scales and the aspect ratios. Possible applications include light-emitting diodes, diode lasers, and other electro-optical devices [1–14]. Extensive investigation has been done on the fabrication and the properties of 1D nanocrystallites, especially hollow nanotubes [9, 15] and solid nanorods and nanowires [2–8, 11–14]. Recently, 1D nanobelts [1, 16, 17], different from the tubes, rods, and wires, have been successfully fabricated through the techniques of different thermal evaporations [16] and wet solution [17]. Generally, the belt-like semiconductors with a well-defined cross section and perfect crystallinity have proven to be an ideal system for the understanding of dimensional confinement and the applications of technologically related nanoscale devices.

Semiconductor ZnO with a wide band gap of 3.37 eV and a large exciton binding energy of 60 meV has been widely used in the areas of light-emitting diodes, optical modulator waveguides, high-efficiency solar cells, and gas sensors [10, 16, 18, 19]. Based on the substantial technological and some potential applications, much effort has been invested in developing fabrication techniques for the growth of ZnO from single crystal to films, along with controlling the geometric configurations, shapes, complex architecture, and fashioning of ZnO nanocrystallites [18–23]. The well-aligned ZnO nanowires were fabricated with both wet solutions [18] and vapor transport methods on various substrates, such as an Au-coated sapphire substrate at 880 °C [10], a nickel monoxide catalyzed alumina substrate through a simple metal-vapor deposition method at 450 °C [20], and a silicon wafer at 400–500 °C through a metal-catalyst-free growth model from an organometallic precursor [21, 22]. To date, many belt-like nanocrystallites have been fabricated since the report of semiconducting transition-metal oxides prepared through the thermal evaporation route, while aligned nanobelt arrays were less reported. In this paper, we report that large-scale aligned semiconductor ZnO nanobelts can be fabricated at a relevant low growth temperature (450 ± 10 °C) through an easily conducted evaporation route from metallic zinc plates. The photoluminescence (PL) property of single ZnO nanobelts was also investigated.

2 Experimental

In typical experiments, three pieces of zinc plate (20 mm × 10 mm × 0.5 mm) were set into an alumina boat. Then the alumina boat was semi-covered with an alumina plate (12 mm × 10 mm × 1 mm) with the two ends of the boat open. After that, the boat was transferred into a quartz tube (800 mm × 35-mm diameter) and subjected to flowing Ar (100–200 sccm) for 10 min. For the oxidization of zinc, there was a hole of about 1-mm diameter left at the inlet of the quartz tube for the leakage of humid air (less than 1% pro-

✉ Fax: +86-551/3603987, E-mail: qyang@ustc.edu or qyoung@ustc.edu.cn

portion with more than 30% relative humidity) at 30°. The tube was heated from room temperature to 450 ± 10 °C in 40 min and maintained for 3–5 h with constant Ar flowing. The furnace was then allowed to cool to room temperature naturally, and a white product was observed in the boat.

The ZnO nanobelt array has been structurally characterized using SEM [FE-SEM (field emission scanning electron microscopy), JEOL JSM-7500B at 10 kV or ESEM (environmental scanning electron microscopy), FEI XL30 at 10 to 20 kV], TEM (transmission electron microscopy) and high-resolution (HR) TEM (JEOL 2010 at 200 kV), EDS (energy-dispersive X-ray spectroscopy, Oxford INCA300), and XRD (X-ray diffraction, Philips X'pert). The room-temperature PL spectra of the single nanobelts were measured on a LABRAM-HR spectroscope, excited with a He–Cd laser source of 325-nm line.

3 Results and discussion

A typical survey SEM image of ZnO sample growth in the alumina boat demonstrates a fashioning of a nanobelt array, shown in Fig. 1a. EDS analysis of the samples indicated that the belts consist of oxygen and zinc, with a relatively large percentage of zinc attached to the un-reacted zinc in the boat (Fig. 1b). A high-resolution side-view SEM image of the belt array is shown in Fig. 1c, where the size of an individual belt is observed to be at least 80 micron in length and 100 nm in width. Most of the belts have an aligned direction with uniform size, and some of them have several bends along the growth direction. XRD recorded on the belt array can be readily indexed according to the wurtzite ZnO crystal structure (Fig. 1d). The relative intensity of the (0002) plane is more intense when compared to the corresponding reflex in the standard ZnO XRD pattern, which indicates that the ZnO nanobelt array may have a preferential orientation along the [0001] direction. XRD also shows the existence of metallic zinc, resulting from the un-oxidized raw material.

A further structure study of the as-prepared nanobelts is demonstrated in Fig. 2. TEM images confirm that the samples have a belt-like morphology with about 100 nm in width from a randomly selected region. From the bends of the belts, we can easily find that the thickness of the belts is close to 30 nm (Fig. 2a). A typical selected-area ED pattern (inset in Fig. 2b) taken from an individual thin nanobelt indicates that the belt grows along the [0001] direction, which is in agreement with the

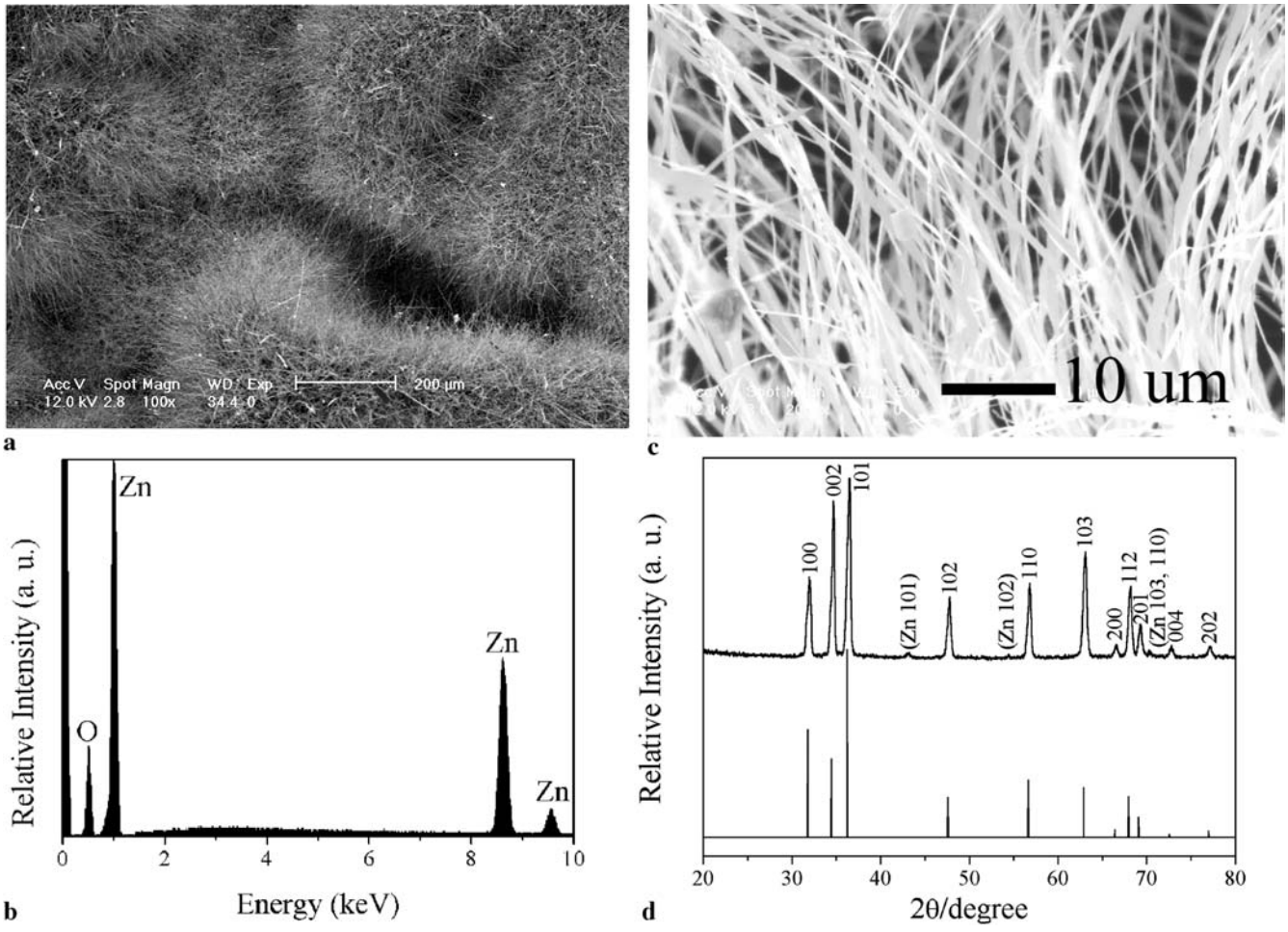

FIGURE 1 **a** Typical survey SEM image of the ZnO sample fabricated on the un-reacted metallic zinc; **b** the corresponding EDS of the samples; **c** high-magnification SEM image showing that the aligned nanobelts grew in an array fashion; **d** XRD pattern of the nanobelt array with a preferential orientation of [0001] (*top*) and the standard ZnO XRD pattern (JCPDS card no. 89-0511, *bottom*)

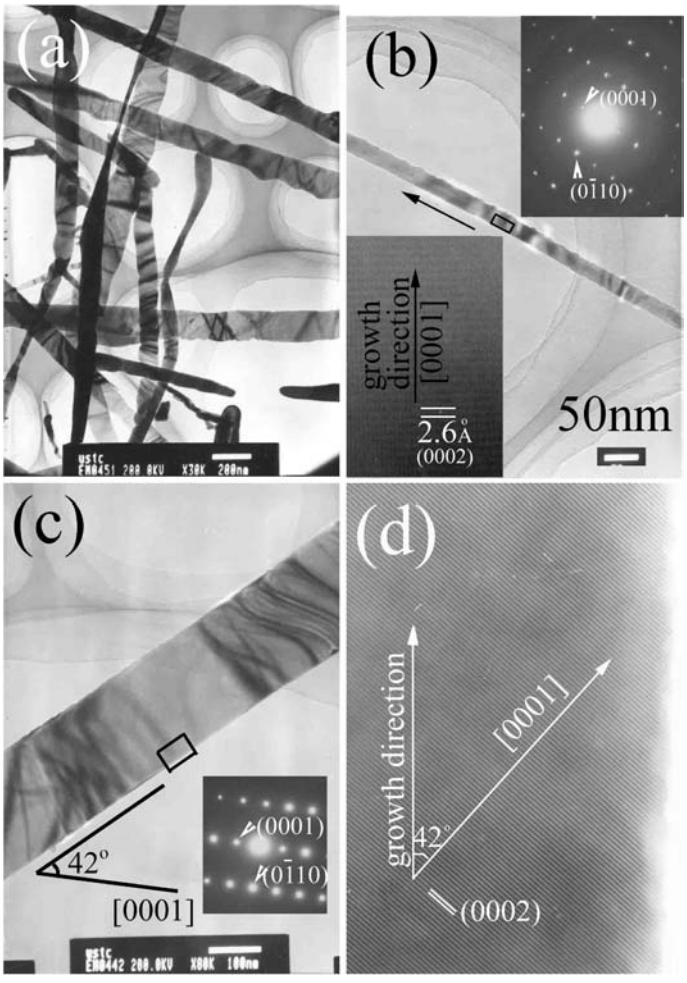

FIGURE 2 **a** TEM image of the ZnO nanobelts with about 30 nm in thickness from the bends; **b** a typical belt grown along the [0001] direction with corresponding ED pattern (projected along the [2$\bar{1}\bar{1}$0] axis) and HRTEM image; **c** and **d** the nanobelt grown along the direction perpendicular to the (01$\bar{1}$2) plane

XRD results shown in Fig. 1d. Figure 2b gives a HRTEM image of the individual belt, which presents a wurtzite ZnO (0002) lattice fringe of $\sim$ 2.6 Å. The result is similar to the value reported by Wang and others [16, 18–24]. Some interesting cases of other growth directions different from the [0001] axis can also be found for the belts. Figure 2c and d show that a nanobelt grows along the direction perpendicular to the (01$\bar{1}$2) crystalline plane, since the measured angle of 42° between the growth direction and the [0001] axis is close to the calculated angle of 42.75° between the two planes of (0001) and (01$\bar{1}$2) in wurtzite ZnO.

The growth of the nanobelts results from an evaporation of metallic zinc with an oxidation and deposition on an early-formed solid ZnO layer (Fig. 3). This solid ZnO layer formed at such an early temperature-elevating stage serves as the substrate for the growth of the nanobelts. It is noted that the growth of the belts may not be deduced from the known vapor–liquid–solid (VLS) growth model for the formation of a 1D structure [7, 25–27]. Although the asset reaction temperature of 450 ± 10 °C is favorable for the oxidation of the source zinc to form solid ZnO phase (see image in Fig. 3), and the temperature above the melting point of zinc (419.6 °C) may provide the other two phases (liquid zinc droplets and zinc vapor) for the growth of ZnO nanobelts in the regime of the VLS model, we did not observe any zinc droplets on the tips of the belts (see Fig. 2). The experimental observation along with the above characterization suggests that the nanobelts are mainly fabricated using a simple evaporation model. It is also noted that the trace of leaked humid air is favorable for the formation of the nanocrystals at such a relative low temperature, which is mainly due to the mass transfer of water [1]. When leaked dry air was used for comparison, we did not obtain well-aligned nanobelts. Meanwhile, the intrinsic anisotropic wurtzite structure of ZnO is also favorable for the 1D growth [3, 4, 10, 16, 18–24]. Some produced bent nanobelts may result from the switching of the growth direction in the process, reported for that of SiC [28].

The room-temperature PL of an individual nanobelt is demonstrated in Fig. 4. The intense peak at 387.5 nm (3.20 eV) is due to the near-band-edge emission of the wide-band-gap ZnO. A very low intense broad visible green emission centered at about 514 nm can be detected, which is often connected with the structure defects, ionized vacancies, or impurities [21–23, 29–31]. According to Vanheusden et al.'s work [32], the green emission at 510 nm (2.43 eV) was due to the recombination of the photogenerated hole with the singly ionized oxygen vacancy. Recently, Fu and co-workers' calculation also suggested that the green emission at 520 nm (2.38 eV) in ZnO was attributed

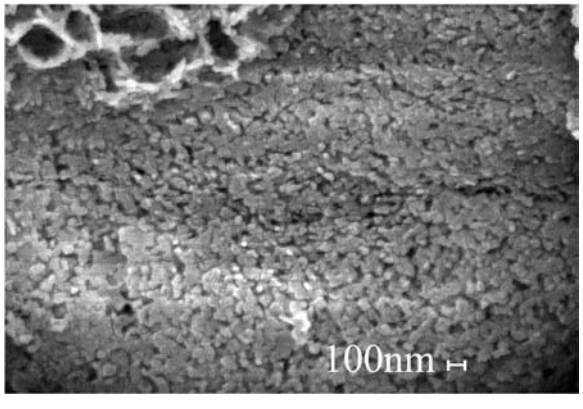

FIGURE 3 A layer of ZnO can be formed on the surface of zinc plate when the reaction occurred in 5 min

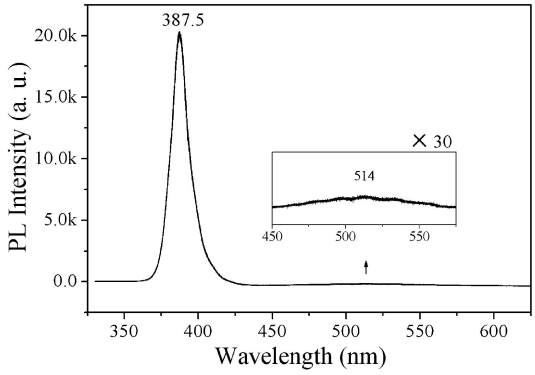

FIGURE 4 The room-temperature PL spectrum of an individual ZnO nanobelt

to the antisite oxygen [33]. To know more about PL of the single nanobelts; at least dozens of single nanobelts have been investigated at room temperature. It is found that the intense band-edge emission of these single belts is generally observed in the range of 384 to 391 nm. The PL spectra from another two typical single nanobelts are shown in Fig. 5. In addition to the intense band-edge emission (at 388.3 and 391 nm) and the weak green emission at 514 nm, a low shoulder emission centered at about 421 nm (2.94 eV) is observed. This violet emission can be attributed to the defect of the interstitial zinc Zn_i (2.90 eV) in ZnO based on a defect-level calculation [33]. The large intensity ratio between the near-band-edge emission and the defect luminescence implied that the as-prepared nanobelts have good crystallinity.

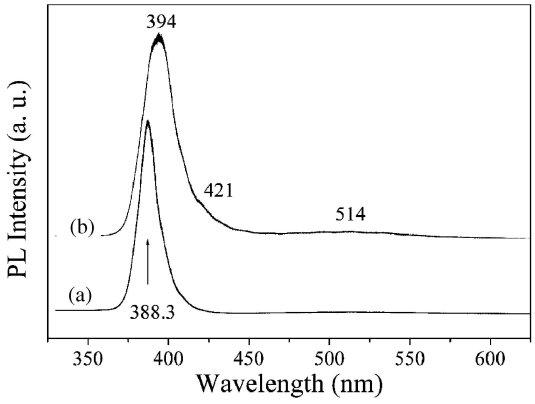

FIGURE 5 The PL spectra of another two typical single ZnO nanobelts

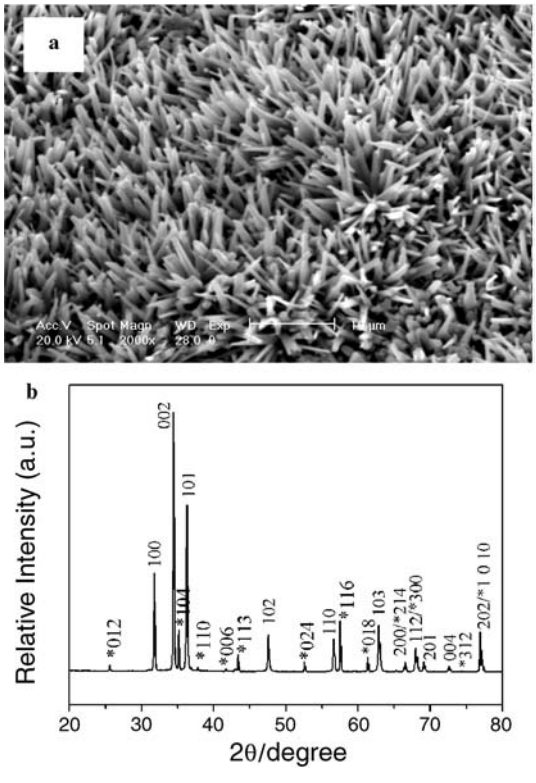

FIGURE 6 **a** Nanorod array on the alumina cover plate can be produced in the process; **b** the corresponding XRD pattern suggests wurtzite ZnO with a [0001] preferential growth (∗: Al_2O_3)

Aligned nanorods (Fig. 6a), different from the belt structure, are also obtained by growing on the alumina cover plate in the same process. XRD patterns (Fig. 6b) suggest that the rod array is oriented in the [0001] direction, similar to the grown aligned nanobelts. The phenomenon of different growth morphologies related to growth sites has been observed previously, which is mainly due to the various mass transfers in the process.

4 Conclusion

In summary, we have demonstrated a simple evaporation route for the growth of an aligned wurtzite ZnO nanobelt array using the oxidization of metallic zinc at a relatively low temperature ($450 \pm 10\,^{\circ}C$) under ambient pressure. Structural characterization with XRD, SEM, and TEM reveals that the as-prepared nanobelt array mostly grew along the [0001]-axis direction with a single-crystal nature. The PL spectra of the individual nanobelts demonstrate that the belts have an intensive and sharp band-edge emission and a very weak and broad green-emission band centered at about 514 nm. In the same process, well-aligned nanorods deposited on the alumina cover plate were also fabricated. The growth of the 1D ZnO nanostructures can be explained by a simple evaporation model and the intrinsic anisotropic property of wurtzite ZnO. It is believed that the simple and easily conducted fabrication route at low temperature and ambient pressure provides a short cut for the wide applications of 1D nanostructures in technology.

ACKNOWLEDGEMENTS The authors gratefully acknowledge the support of this project by the Anhui Provincial Natural Science

Foundation (No. 3044901) and National Natural Science Foundation of China. We thank Profs. Shuhong Yu and Shuyuan Zhang for discussions.

REFERENCES

1 M.P. Zach, J.T. Newberg, L. Sierra, J.C. Hemminger, R.M. Penner: J. Phys. Chem. B **107**, 5393 (2003)
2 F. Favier, E. Walter, M. Zach, T. Benter, R.M. Penner: Science **293**, 2227 (2001)
3 X.G. Peng, L. Manna, W.D. Yang, J. Wickham, E. Scher, A. Kadavanich, A.P. Alivisatos: Nature **404**, 59 (2000)
4 J.G. Wen, J.Y. Lao, D.Z. Wang, T.M. Kyaw, Y.L. Foo, Z.F. Ren: Chem. Phys. Lett. **372**, 717 (2003)
5 H.J. Shin, R. Ryoo, Z. Liu, O. Terasaki: J. Am. Chem. Soc. **123**, 1246 (2001)
6 S. Park, S. Kim, S. Lee, Z.G. Khim, K. Char, T. Hyeon: J. Am. Chem. Soc. **122**, 8581 (2000)
7 Q.Y. Lu, J.Q. Hu, K.B. Tang, Y.T. Qian, G.E. Zhou, X.M. Liu, J.S. Zhu: Appl. Phys. Lett. **75**, 507 (1999)
8 Q. Yang, K.B. Tang, C.R. Wang, Y.T. Qian, S.Y. Zhang: J. Phys. Chem. B **106**, 9227 (2002)
9 J. Zhang, L.D. Sun, C.S. Liao, C.H. Yan: Soc. Chem. Commun. 262 (2002)
10 M.H. Huang, S. Mao, H. Feick, H.Q. Yan, Y.Y. Wu, H. Kind, E. Weber, R. Russo, P.D. Yang: Science **292**, 1897 (2001)
11 D.W. Wang, H.J. Dai: Angew. Chem. Int. Edit. **41**, 4783 (2002)
12 H.J. Dai, E.W. Wong, Y.Z. Lu, S.S. Fan, C.M. Lieber: Nature **375**, 769 (1995)
13 U. Banin, O. Millo: Annu. Rev. Phys. Chem. **54**, 465 (2001)
14 M.A. El-Sayed: Acc. Chem. Res. **34**, 257 (2001)
15 M. Terrones: Annu. Rev. Mater. Res. **33**, 419 (2001)
16 Z.W. Pan, Z.R. Dai, Z.L. Wang: Science **291**, 1947 (2001)
17 M.S. Mo, J.H. Zeng, X.M. Liu, W.C. Yu, S.Y. Zhang, Y.T. Qian: Adv. Mater. **14**, 1658 (2002)
18 L. Vayssieres: Adv. Mater. **15**, 464 (2003)
19 D.C. Reynolds, D.C. Look, B. Jogai, J.E. Hoelscher, R.E. Sherriff, M.T. Harris, M.J. Callahan: J. Appl. Phys. **88**, 2152 (2000)
20 S.C. Lyu, Y. Zhang, H. Ruh, H.J. Lee, H.W. Shim, E.K. Suh, C.J. Lee: Chem. Phys. Lett. **363**, 134 (2002)
21 W.I. Park, G.-C. Yi, M. Kim, S.J. Pennycock: Adv. Mater. **14**, 1841 (2002)
22 J.-J. Wu, S.-C. Liu: Adv. Mater. **14**, 215 (2002)
23 Y.B. Li, Y. Bando, T. Sato, K. Kurashima: Appl. Phys. Lett. **81**, 144 (2002)
24 J.C. Johnson, H.Q. Yan, P.D. Yang, R.J. Saykally: J. Phys. Chem. B **107**, 8816 (2003)
25 Y.H. Yang, S.J. Wu, H.S. Chiu, P.I. Lin, Y.T. Chen: J. Phys. Chem. B **108**, 846 (2004)
26 Y.Y. Wu, P.D. Yang: J. Am. Chem. Soc. **123**, 3165 (2001)
27 X.F. Duan, C.M. Lieber: J. Am. Chem. Soc. **122**, 188 (2000)
28 Z.L. Wang, Z.R. Dai, R.P. Gao, Z.G. Bai, J.L. Gole: Appl. Phys. Lett. **77**, 3349 (2000)
29 P.D. Yang, H.Q. Yan, S. Mao, R. Russo, J. Johnson, R. Saykally, N. Morris, J. Pham, R.R. He, H.J. Choi: Adv. Funct. Mater. **12**, 323 (2002)
30 J.Q. Hu, Q. Li, N.B. Wong, C.S. Lee, S.T. Lee: Chem. Mater. **14**, 1217 (2002)
31 V.A.L. Roy, A.B. Djurisic, W.K. Chan, J. Gao, H.F. Lui, C. Surya: Appl. Phys. Lett. **83**, 141 (2003)
32 K. Vanheusden, W.L. Warren, C.H. Seager, D.R. Tallant, J.A. Voigt, B.E. Gnade: J. Appl. Phys. **79**, 7983 (1996)
33 B. Lin, Z. Fu, Y. Jia: Appl. Phys. Lett. **79**, 943 (2001)